In Situ X-Ray Scattering Study of Incipient Formation of Porous Silicon

Hoydoo You[1], Kegang Huang[1], S.S. Yoo[1], and Zoltan Nagy[2]

[1]Materials Science Division, Argonne National Laboratory, Argonne, IL 60439
[2]Materials Science and Chemical Technology Divisions, Argonne National Laboratory, Argonne, IL 60439

Materials Science Division
Argonne National Laboratory
Argonne, IL 60439

December 1995

/jc

Distribution:

1-2. M. J. Masek
3. B. D. Dunlap
4. P. A. Montano
5. F. Y. Fradin
6. R. Gottschall
7. Editorial Office
8. Authors

Submitted as a conference paper to International Symposium on Advanced Luminescence Materials 188th Meeting of the Electro-Chemical Society, Chicago, IL , Oct. 8-13, 1995.

This work is supported by the Division of Materials Sciences, Office of Basic Energy Sciences of DOE, under contract No. W-31-109-ENG-38.

IN SITU SYNCHROTRON X-RAY SCATTERING STUDY OF INCIPIENT FORMATION OF POROUS SILICON

Hoydoo You, Kegang Huang, and S.S. Yoo
Materials Science Division

Zoltán Nagy
Materials Science and Chemical Technology Divisions
Argonne National Laboratory, Argonne, Illinois 60439, USA

ABSTRACT

The incipient formation of porous silicon at the solution/silicon interface was examined in situ using synchrotron x-ray scattering techniques. The measurements were performed in a transmission x-ray/electrochemistry cell with p^+ type silicon single crystals. The structure of pores near the interface is determined from x-ray reflectivity and diffuse-scattering measurements. We found an interfacial layer with tapered cylindrical pores, followed by a layer of uniform porosity with increased branching with depth. For our conditions, the porosity was around 50%, and the pore diameter was about 50 to 70 Å.

1 INTRODUCTION

It has been widely recognized that porous silicon, and porous semiconductors in general, are potentially very important materials for future industrial applications because of their luminescence at visible frequencies. In addition they can be easily manufactured into existing silicon-based electronic devices with lithographic fabrication and anodic dissolution techniques [1, 2]. More recently, a study of electrochemiluminescence in formic acid solution has further stimulated possible applications of porous silicon fabricated on silicon substrates in future devices [3]. Despite the wide recognition of importance of these materials, relatively little attention was given to and little is known about the incipient stages of the anodic dissolution process. This motivated us to perform an in situ x-ray scattering investigation of solution/silicon single crystal interfaces.

Applications of x-ray scattering techniques for in situ investigation of liquid/solid interfaces has become increasingly popular in recent times because the

availability of bright synchrotron x-ray sources. Several previous studies of metal/solution interfaces have proven that the technique is very powerful for in situ determination of microscopic level details. In particular, it has been shown that a transmission geometry x-ray/electrochemical cell [4] is advantageous for examining electrode surfaces near critical angles and at large Bragg angles under nearly ideal electrochemical conditions. The unrestricted accessibility of x-rays in this cell from near zero to large angles was critical in obtaining details about the interfaces as we will discuss below.

Several x-ray-diffraction studies of porous silicon in air were carried out in the past. For example, small angle scattering was used to study the size of the silicon particles resulting from the oxidation of porous silicon layers [5], and diffuse scattering was used to study crystallinity and strain in porous silicon [6]. Both studies were performed ex situ and focused on the structural properties of aged or oxidized samples of porous silicon. Transmission electron microscopy studies were also carried out [7, 8]. The pore size for p-type silicon was estimated to be as small as 30 Å in all these studies. If this is indeed the size range, x-ray scattering is the only viable in situ technique for examining these pores in direct contact with solution.

2 X-RAY REFLECTIVITY

In this section we will introduce the basic aspects of x-ray reflectivity to provide a basis for our subsequent discussion (Sec. 4). A beam of x-rays impinging on an interface formed by two adjacent media, like any other electromagnetic wave, follows the laws of classical optics, in particular, Snell's law and Fresnel's law of reflectivity. One parameter in these optical considerations is the difference between the index of refraction and unity. For x-rays, this difference is a small negative number while for visible light it is a large positive number. Consequently, at angles below the critical angle of incidence with respect to the interface, visible light exhibits total internal reflection (total reflection back to the dense medium), while x-rays exhibit total external reflection (total reflection back to the sparse medium). The critical angle (θ_c) is related to the indices of refraction of the two media as $\cos\theta_c = n'/n$, and it is typically smaller than 1° for x-rays. One can therefore write the equation for Fresnel reflectivity for a sharp interface as

$$R_F = \left| \frac{\sin\theta - \sqrt{\sin^2\theta - \sin^2\theta_c}}{\sin\theta + \sqrt{\sin^2\theta - \sin^2\theta_c}} \right|^2 \qquad (1)$$

where the angle of incidence (θ) and θ_c are measured with respect to the interface. For $\theta \leq \theta_c$, the value of $\sqrt{\sin^2\theta - \sin^2\theta_c}$ becomes an imaginary number and the reflectivity is unity. For $\theta \gg \theta_c$, the reflectivity falls off with $(\sin\theta_c/\sin\theta)^4$. It is

customary to express the measured reflectivity data in units of momentum transfer, $Q = 4\pi \sin\theta/\lambda$, and this unit will be used throughout this paper.

Equation (1) is accurate when the interface is sharp, that is, when the interface width is small compared to the wavelength of the x-rays. For a rough interface, the electron density perpendicular to the interface changes gradually, and the width of the interfacial region becomes larger than the wavelength of the x-rays. For these conditions, the reflectivity relation is

$$R(Q) \cong R_F \left| \int \frac{d\rho(z)}{dz} e^{iQz} dz \right|^2 \tag{2}$$

For an ideally sharp interface, the function $\rho'(z)$ is a δ-function, and the reflectivity follows Fresnel's law as written in equation (1). Consequently, the reflectivity falls off with increasing angle of incidence as $1/Q^4$. For a non-ideal interface $\rho'(z)$ has a finite width, and the reflectivity falls off faster than $1/Q^4$.

3 EXPERIMENTAL

The x-ray experiments were performed with a standard four-circle diffractometer at beamline X6B of the National Synchrotron Light Source at Brookhaven National Laboratory. A monochromatic beam of x-rays with wave length of 1.056 Å was partially focused by a toroidal mirror at a reflecting angle of 5.5 mrad. At this reflecting angle the focal point was at a point 12 m behind the sample position. This configuration was chosen to deliberately decrease the convergence of the beam and to achieve high momentum resolution without loosing too much flux. The cell geometry is shown schematically in Fig. 1. The x-ray beam enters from one side of the cell through a Teflon-coated Kapton-film window. It passes through the solution, scatters from the sample surface, and exits through a window at the other side of the cell.

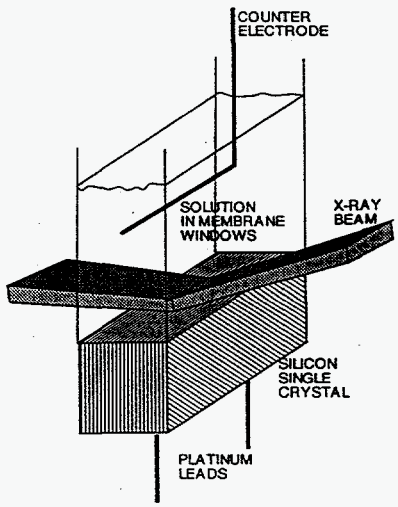

Figure 1: A schematic diagram of x-ray/electrochemical cell used in this study.

P-type silicon single crystals with a resistance of 0.015 Ω/cm were used in these experiments. The (100) surface of the crystals was commercially polished, and they were cut to a size of $3 \times 3 \times 20$ mm. The area exposed to the solution was 3×10 mm,

and the roughness of the sample surface was 2 to 3 Å root-mean-square (rms). Two platinum wires were pressed against the back of the sample for electrical contacts. The platinum wire counter electrode was located approximately 10 mm directly above the surface.

The silicon crystal was cleaned ultrasonically in three steps: in acetone, in alcohol, and in distilled water, for 5 to 10 minutes each, before the assembly of the cell. The cell was then filled with test solution and moved to the diffractometer. Two types of test solutions were used, namely, HF:H_2O=1:1 and HF:H_2O:C_2H_5OH=1:1:2. The anodic dissolution was carried out under constant current conditions at current densities between 10 and 200 mA/cm^2. The charge passed during a single dissolution step between x-ray measurements was varied from 90 μC (dissolution of $\sim$1.5 Å of solid silicon) to 150 mC (dissolution of $\sim$2500 Å of solid silicon). We found that the alcohol-containing solution yielded a more reproducible and uniform porous layer over the surface. In this paper, the discussion will be limited to the results taken with alcohol-containing solutions.

4 RESULTS AND DISCUSSIONS

In one experiment, we measured the reflectivity before and ($\sim$30 minutes) after the introduction of solution into the cell. The two reflectivity scans are shown in Fig. 2 in a log-log plot. The critical angles for the two conditions are different: the critical angle for the air/silicon interface is 0.033 Å^{-1}, while that for the solution/silicon interface is 0.025 Å^{-1}. The reason for this change is the reduction of the density contrast at the interface. Furthermore, the reflected intensity below the critical angle is smaller than unity for the solution/silicon interface because of the attenuation of x-rays. The 3-mm-thick solution layer attenuated the x-ray beam by a factor of $1/e$.

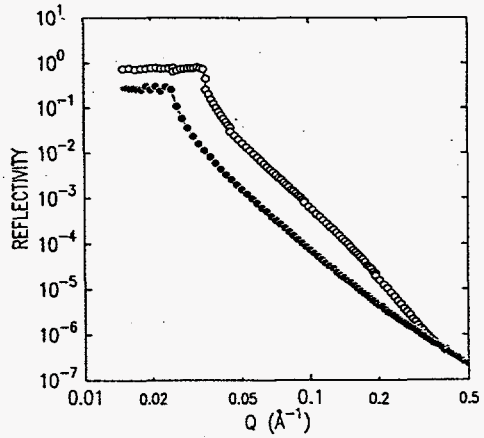

Figure 2: Reflectivity scans before (open circles) and after (solid circles) introduction of HF solution.

For large Q, the reflectivity of the air/silicon interface falls off considerably faster than that of the solution/silicon interface. In other words, the solution/silicon interface is considerably sharper than the air/silicon interface. The increased sharpness of the silicon surface after the introduction of the solution is evidence for the chemical dissolution of the silicon oxide, which is always present at the air/silicon

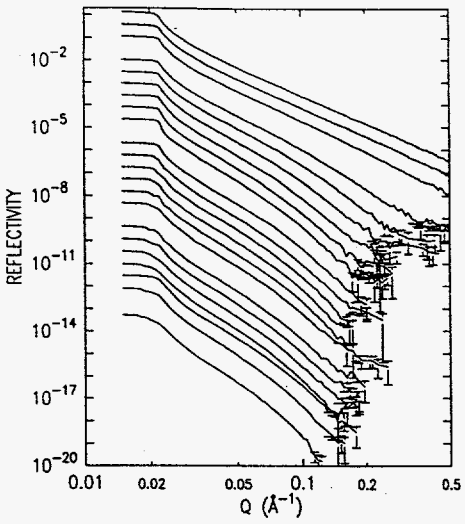

Figure 3: A series of reflectivity scans measured during the short pulse measurements. See the text for details.

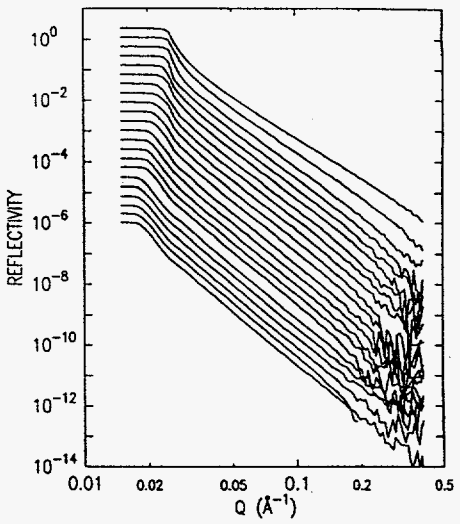

Figure 4: A series of reflectivity scans measured during the long pulse measurements. See the text for details.

interface. The dissolution of silicon oxide in contact with the solution was completed within a few tens of minutes. Once the chemical dissolution of existing oxide was completed, no further change in the reflectivity occurred for many hours, suggesting that dissolution of silicon in HF solution is nonexistent or very slow as long as the silicon remains at open circuit.

We carried out two series of reflectivity measurements during anodic dissolution: one after a varying number of pulses of short duration (0.3 mC) were applied, and another after a varying number of pulses of long duration (7.5 mC). The current density was 10 mA/cm^2 for both cases. Since our sample surface was 0.3 cm^2 and the dissolution occurs with a 2e$^-$/Si process [10], the 0.3 mC dissolution pulses are equivalent to the dissolution of one unit cell height of solid (not porous) silicon (i.e., 5.4 Å), while the 7.5 mC dissolution pulses are equivalent to the dissolution of 135 Å of solid silicon.

The short-pulse scans are shown in Fig. 3. Each successive scan is offset for display purposes. The top scan was carried out before any anodic dissolution, and it is close to that of an ideally sharp interface. The subsequent scans were made after the application of a successively increasing number of dissolution pulses resulting in the dissolution of the equivalent of solid silicon layers ranging from approximately 15 to 600 Å, for a grand total of 4,600 Å.

During the short-pulse experiments, the useful length of the scans decreases as the total dissolution amount increases, because an increasing number of data points fall below the background level at large scattering vectors. The reflectivity scans bend down, which is indicative of a Gaussian rough surface [11]. The larger

the Gaussian width of the interface, the faster the reflectivity drops to the background level. The continuous increase of the interfacial width indicates a random dissolution process at the interface. This is analogous to a random growth process [12] where the width of the interface continuously increases as the deposition amount increases. In these experiments, we find a continuous roughening of the interface, but we have no definite evidence of pore formation. We may not form pores because the potential does not become positive enough during the short pulses, or because a sharp "pore tip" cannot form during the short pulses [8, 10].

The reflectivity scans obtained for the long-pulse scans are shown in Fig. 4. These scans were also offset for display purposes. The top two scans were carried out before any anodic dissolution. The subsequent scans were made after the application of a successively increasing number of dissolution pulses resulting in the dissolution of the equivalent of solid silicon layers ranging from approximately 135 to 2,500 Å, for a grand total of 24,000 Å.

For the long-pulse experiments, all the scans are linear for angles larger than the critical angle, and the slope of the reflectivity scans changes during the first few successive dissolutions but remains constant thereafter. In other words, the interface density profile reaches a steady state functional form at a critical dissolution depth (~300 Å of solid silicon for this particular set of data). This observation indicates the existence of an interfacial region where the density gradually changes, followed by another layer where dissolution in excess of a critical depth does not significantly alter the density profile any more. Furthermore, this observation also indicates that the interface density profile should follow a power law, $\rho(z) \sim z^{2\alpha}$. Since the deviation from Fresnel reflectivity is due to the roughness of the interface, we can use the power law of the interface density profile to modify Eq. (2), and to obtain the reflectivity equation as

$$R(Q) \cong R_F \left| \int \left(z^{2\alpha}\right)' e^{iQz} dz \right|^2 \approx Q^{-4(1+\alpha)} \tag{3}$$

where the exponent α is a positive number. This form of the reflectivity equation predicts a straight line on a log-log scale, from the slope of which the exponent, α, can be determined. In Fig. 4, the exponent changes from zero (<0.01) for the top reflectivity scan to 0.35 for the scans taken after the critical dissolution depth. The critical angle is well defined for all the scans, and it decreases continuously as the total dissolution amount increases. The critical angle of the top two scans (zero porosity) is 0.025 $Å^{-1}$, and it decreases to 0.018 $Å^{-1}$ for the last scan. Since $\theta_c^2 \sim \Delta\rho(z)$, the porosity ($p_c$) of silicon can be estimated from the measured critical angles as $p_c = 1 - \theta_c^2/0.025^2$. For example, the porosity of the last scan is approximately 52%. This porosity is averaged over a depth of 1.4 μm, which is the penetration depth of x-rays at the critical angle.

Two possible pore distribution models consistent with the power-law density profile are schematically shown in Fig. 5: (a) tapered pores with relatively uniform

length across the sample surface, and (b) pores with uniform radius and a length distribution matching the overall power-law interfacial-density profile. The reflectivity data are consistent with either possibility or with any combination of them. Therefore, additional measurements were made for diffuse scattering around the Bragg reflections to determine which model is closer to the real structure of the pores.

Diffuse scattering around a Bragg peak provides information about the shape and density of the pores, while the reflectivity scans provided information on the near-interface density profile normal to the interface. The theoretical derivation of the relation between the pore distribution and the shape of the diffuse scattering curve is beyond the scope of this paper and readers are referred to Ref. [13].

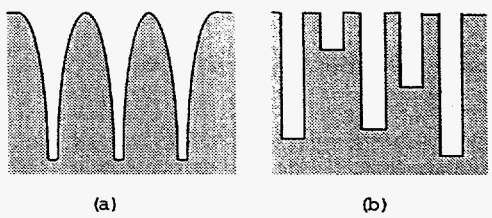

Figure 5: Two possible pore distributions consistent with the reflectivity scans.

Three-dimensional iso-intensity contours are shown for four Bragg reflections in Fig. 6, and typical θ and θ-2θ scans through one Bragg reflection are shown in Fig. 7. In the latter figure, the solid lines represent data taken before anodic dissolution (zero porosity), and the open circles represent data taken at the critical dissolution depth (i.e., when the interface density profile reaches a steady state functional form).

The shoulders (open circles) observable in Fig. 7(a) are present on every scan through the peaks shown in Fig. 6. When pores exist in single crystals, the diffuse scattering from them is replicated throughout all the Bragg reflections in the reciprocal space as shown in Fig. 6. Therefore, the difference between the open circles and the solid line in Fig. 7(a) represents the true diffuse scattering from a set of pores existing in the single crystal silicon. This difference is shown in the

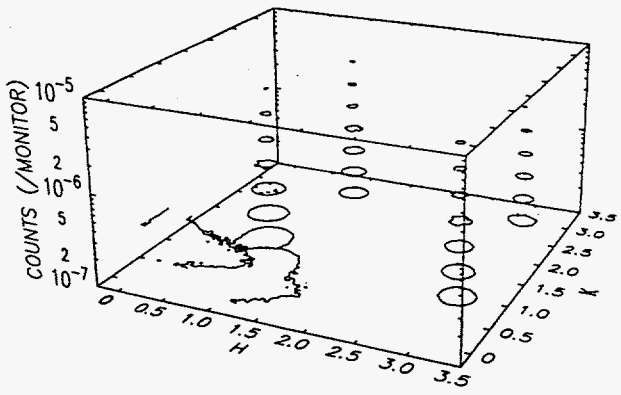

Figure 6: An iso-intensity contour plot of diffuse scattering around four Bragg reflections.

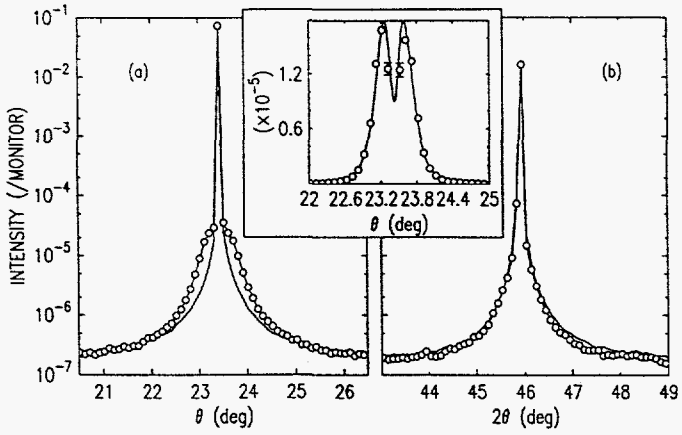

Figure 7: Diffuse scattering around (004) reflection; (a) θ-scan and (b) θ-2θ scan.

inset of Fig. 7. From this, we can deduce the size and shape of the pores. Curve fitting of the data to the porous structure model [13] gives a pore diameter in the range of 50 to 70 Å (the solid line in the inset of Fig. 7 shows the quality of the fit). Furthermore, the diffuse scattering shown in the inset (scan parallel to the surface) is independent of rotation of the sample about the surface normal. From this fact we can conclude that the in-plane shape of the pores is circular.

There are no shoulders on the θ-2θ scan (scan normal to the surface) taken at the critical dissolution depth [Fig. 7(b)]. This absence of diffuse scattering originating from the pores in the θ-2θ scan indicates that the pores are elongated normal to the surface and their diameters are slowly changing over long length scales. If there were a sufficient number of pores whose diameters changed abruptly at the end of the pore as shown in Fig. 5(b), the abrupt changes in the electron density would have produce significant diffuse scattering in the θ-2θ scan. This implies that the pore shape with smoothly changing radius shown in Fig. 5(a) is more consistent with our data.

Numerous previous studies [10] suggest that (i) the pores grow preferentially along the (100) crystallographic direction, (ii) the porosity is independent of pore depth, and (iii) the average pore size is considerably larger for n-type silicon than for p-type. We find these suggestions consistent with our measurements. (i) The direction of the pore formation is perpendicular to the surface, at least for the initial stage (<300 Å). (ii) The intensity of the diffuse scattering shown in the inset of Fig. 7 increases proportionally to the total amount of charge transfer, while the shape of the diffuse scattering is unchanged. The overall average pore diameter and the average porosity are unchanged as the thickness of the porous silicon layer increases, except for the interface region (<300 Å). In the near surface region, of course, the density changes with a power law as indicated by the reflectivity scans. (iii) We observed 50~70 Å average pore diameters for our p-type samples, while

the pore diameters for n-type samples are in the micron range.

While it is difficult to study the microscopic structure of p-type porous silicon crystals, there have been TEM studies of n-type silicon [7, 8]. More recently, a computer simulation study was reported, also for n-type porous silicon, predicting a microscopic model [10]. Since these studies were for n-type silicon, our measurements can not be directly compared to their predictions. Nonetheless, such a comparison is still interesting. Both the TEM and the computer studies divide the porous structure into three regions: (i) the interfacial region, (ii) the porous body region, and (iii) the pore tip region. For the interface region, the TEM studies find narrow pores like a collection of bottle necks, while the computer studies find that the number of pores is substantially higher and the porosity is also higher than in the body region, and that the porosity rapidly decreases to that of the body region. Both studies indicate that there is a fairly uniform porosity region, called a body region and there is a tip region where the pore density rapidly diminishes. The computer simulation studies [10, 14] also predicted that the branching is small at the interfacial region but gradually increases as the depth of the porous region increases.

Our reflectivity and diffuse scattering measurements indicate that the pore diameter rapidly changes at the interface region as shown in Fig. 5(a). This agrees with the predicted increased porosity, but it is contrary to the observed bottle-neck shape, possibly because of the different type of silicon used in our study. Our measurements are consistent with the body region found in the above quoted studies, including the increased branching with pore depth. This behavior was also observed (but not presented in this paper) in our diffuse scattering measurements: the diffuse scattering intensity in θ-2θ scans through a Bragg reflection [Fig. 7(b)] is unchanged by the pores for the interfacial region, but the contribution from pores gradually increases as the depth of the porous silicon is increased beyond the critical depth, indicating the development of branches. Our measurement sensitivity is not sufficient to obtain information about the tip region of the porous layer.

5 CONCLUSIONS

We have demonstrated that x-ray scattering techniques can be applied for in situ examination of incipient formation of porous silicon during anodic dissolution. We obtained microscopic information about this process that otherwise would not be easily available. We found that an interfacial layer with funnel-shaped (tapered) pores, followed by a layer of uniform porosity with increased branching with depth. For our conditions, the porosity was around 50%, and the pore diameter was about 50 to 70 Å. This work identifies potential advantages of the use of synchrotron based x-ray scattering techniques for studies of a wide variety of liquid/semiconductor interfaces under electrochemical processing conditions.

This work was supported by the Division of Materials Sciences, Office of Basic Energy Sciences, U.S. Department of Energy, under Contract No. W-31-109-ENG-38.

REFERENCES

[1] P.C. Searson, J.M. Macaulay, and S.M. Prokes, J. Electrochem. Soc., **139**, 3373 (1992).

[2] V.V. Doan and M.J. Sailor, Appl. Phys. Lett., **60**, 619 (1992).

[3] W.H. Green, E.J. Lee, J.M. Lauerhaas, T.W. Bitner, Appl. Phys. Lett., **67** 1468 (1995).

[4] Z. Nagy, H. You, R. M. Yonco, C. A. Melendres, W. Yun, and V. A. Maroni, Electrochim. Acta, **36,** 209 (1991); H. You, C. A. Melendres, Z. Nagy, V. A. Maroni, W. Yun, and R. M. Yonco, Phys. Rev., **B45**, 11288 (1992); H. You, D. J. Zurawski, Z. Nagy, and R. M. Yonco, J. Chem. Phys., **100**, 4699 (1994).

[5] A. Naudon, P. Goudeau, A. Halimaoui, B. Lambert, G. Bomchil, J. Apply. Phys. **75**, 780 (1994).

[6] E. Koppensteiner, A. Schuh, and G. Bauer, V. Holy, D. Bellet, and G. Dolino, Appl. Phys. Lett., **65**, 1504 (1994).

[7] M.W. Cole, J.F. Harvey, R.A. Lux, and D.W. Eckart, Appl. Phys. Lett., **60** 2800 (1992).

[8] X.G. Zhang, J. Electrochem. Soc. **138**, 3750 (1991).

[9] M.G. Berger, R. Arens-Fischer, St. Fronhnhoff, C. Dieker, K. Winz, H. Munder, H. Luth, M. Arntzen and W. Theiss, *Proceedings of the Materials Research Society,* Boston, USA, Nov. 28 – Dec. 2, 1994.

[10] J. Erlebacher, K. Sieradzki, and P.C. Searson, J. Appl. Phys. **76**, 182 (1994) and references therein.

[11] When $\rho'(z)$ has a Gaussian form, $\log R(Q) \approx \log[\exp(-Q^2\sigma^2)/Q^4] = -4\log Q - \sigma^2 10^{(2\log Q)}$. The reflectivity will bend down on a log-log scale, due to the second term. In fact, this bending will occur for any exponential form of $\rho'(z)$.

[12] H. You, R. P. Chiarello, H. K. Kim, and K. G. Vandervoort, Phys. Rev. Lett. **70**, 2900 (1993) and references therein.

[13] H. You, K.G. Huang, and R.T. Kampwirth, Physica B, *Proceedings of the Fourth International Conference on Surface X-ray and Neutron Scattering,* Lake Geneva, WI, USA, June 25-30, 1995.

[14] V.P. Parkhutik, Private communication.